

Estimating and Maximizing Mutual Information for Knowledge Distillation

Aman Shrivastava¹, Yanjun Qi¹, Vicente Ordonez²

¹University of Virginia, ²Rice University
{as3ek, yq2h}@virginia.edu, vicenteor@rice.edu

Abstract

Knowledge distillation is a widely used general technique to transfer knowledge from a teacher network to a student network. In this work, we propose Mutual Information Maximization Knowledge Distillation (MIMKD). Our method uses a contrastive objective to simultaneously estimate and maximize a lower bound on the mutual information between intermediate and global feature representations from the teacher and the student networks. Our method is flexible, as the proposed mutual information maximization does not impose significant constraints on the structure of the intermediate features of the networks. As such, we can distill knowledge from arbitrary teachers to arbitrary students. Our empirical results show that our method outperforms competing approaches across a wide range of student-teacher pairs with different capacities, with different architectures, and when student networks are with extremely low capacity. We are able to obtain 74.55% accuracy on CIFAR100 with a ShuffleNetV2 from a baseline accuracy of 69.8% by distilling knowledge from ResNet50.

1 Introduction

Recent machine learning literature has seen a lot of progress driven by deep neural networks. Many such models that achieve state-of-the-art performance on different benchmarks (Huang and Wang 2018) require large compute and storage capacities. These requirements limit the wider adoption of these models in resource-limited scenarios. To this end, knowledge distillation, as proposed by Hinton *et al.* (Hinton, Vinyals, and Dean 2015), aims to transfer knowledge from a stronger teacher network to a more efficient student network. This allows the student network to outperform an identical model that is trained without the teacher.

In Hinton *et al.* (Hinton, Vinyals, and Dean 2015), distillation was performed by minimizing the Kullback–Leibler divergence between the teacher and the student output logits. Since then, several other output-based knowledge distillation approaches have been developed (Hinton, Vinyals, and Dean 2015; Zhang, Zhu, and Ye 2019; Chen *et al.* 2017; Tian, Krishnan, and Isola 2019). These methods try to match the outputs probabilities of the networks by minimizing a certain distance metric. While another line of work has pursued feature-based distillation (Romero *et al.* 2014; Zagoruyko and Komodakis 2016a; Ahn *et al.* 2019), where

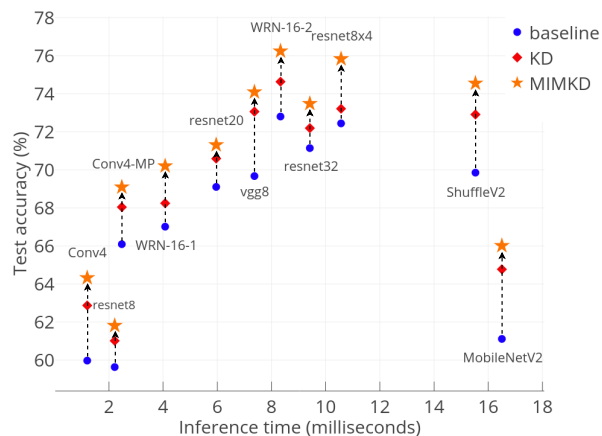


Figure 1: We show the accuracy-efficiency trade-off of various CNN models on the CIFAR100 dataset. Efficiency is measured as the average inference time over a single input. MIMKD provide significant gains over baseline accuracy across a range of models. *Note:* Runtimes were computed on an Intel(R) Xeon(R) Gold 5218 CPU @ 2.30GHz.

additional knowledge transfer is encouraged by minimizing a metric between intermediate network representations of the teacher and the student. Feature-based knowledge distillation has been shown to be valuable and provides useful supervision to the student model to learn more informative representations. However, models with significantly different architectures have distinct data-abstraction flows, and the complexity of the patterns recognized at different depths in the model varies significantly with model architecture (i.e. the number of filters in convolutional layers). Therefore, minimizing a non-parameterized distance metric on the representations imposes an additional structural constraint on student’s training that might not be ideal for knowledge transfer. In this work, we propose a distillation framework that aims to maximize the shared information between the intermediate and final representations from the teacher and the student networks by leveraging a contrastive objective.

Recently, Contrastive Representation Distillation (CRD) (Tian, Krishnan, and Isola 2019) used a Noise Contrastive Estimation based objective (Oord, Li, and Vinyals 2018; Gutmann and Hyvärinen 2010) to transfer structured relational knowledge from the teacher to the student. However, a caveat of this approach is that it requires comparing features from a large number of images simultaneously. In practice, this requires large batches (Chen et al. 2020) or memory banks (He et al. 2020; Wu et al. 2018).

In this paper, we look at knowledge distillation from an information-theoretic perspective. For better distillation, the student needs to generate representations that share maximum information with the representations generated by the teacher. Based on this intuition, we propose Mutual Information Maximization Knowledge Distillation (MIMKD). In previous literature, multiple approaches have been proposed to estimate the mutual information between high-dimensional continuous variables. For instance, In Belghazi et al. (2018), Mutual Information Neural Estimation (MINE) uses a KL-divergence based formulation of mutual information. We observe that MINE can be extended to maximize the mutual information in a contrastive setup. However, in contrast to MINE, we find that a Jensen-Shannon divergence (JSD) based formulation is more stable and the performance is invariant to the number of negative samples – as also demonstrated in Deep InfoMax (Hjelm et al. 2018). Hence, our JSD-based contrastive objective uses only one negative sample as opposed to 16384 used in CRD (Tian, Krishnan, and Isola 2019). This allows us to impose region-consistent local and feature-level constraints as large number of negative samples for intermediate features are not required.

We propose three mutual information maximization objectives between the teacher and student networks: (1) *Global information maximization*, which aims to maximize the shared information between the final representations of networks. This pushes the student network to generate feature vectors that are as rich as the ones generated by the teacher. (2) *Local information maximization*, which pushes the student network to recognize complex patterns from each region of the image that are ultimately useful for classification. This is achieved by maximizing the mutual information between region-specific vectors extracted from an intermediate representation of the student network and the final representation of the teacher network. Finally, (3) *Feature Information Maximization*, which is designed to structurally improve the granular feature-extraction capability of the student by maximizing the mutual information between region-consistent local vectors extracted from intermediate representations of the networks.

We demonstrate that these objectives are more effective than competing methods across a wide range of student-teacher pairs and conduct extensive ablation studies of the effect of each proposed objective. We particularly demonstrate the effectiveness of our method in knowledge distillation across student-teacher network pairs with different capacities, student-teacher network pairs with different architectures, and in the extreme case where student networks are extremely low capacity. We show that MIMKD provides consistently better results across all these testing scenarios.

2 Background and Related Work

In this section, we discuss previous efforts in improving knowledge distillation, and in estimating mutual information which are the key areas of contribution of our work.

Knowledge distillation. The concept of knowledge distillation (KD) was introduced in the works of Buciluă et al. (Buciluă, Caruana, and Niculescu-Mizil 2006) and later formalized for deep neural networks by Hinton et al. (Hinton, Vinyals, and Dean 2015). In knowledge distillation, the goal is to train smaller models that can mimic the performance of larger models. Hinton et al. (Hinton, Vinyals, and Dean 2015) proposed a knowledge distillation method in which the student network is trained using soft labels extracted from teacher networks.

Attention transfer (Zagoruyko and Komodakis 2016a) introduced the idea of transferring intermediate attention maps from the teacher to the student network. Fitnets (Romero et al. 2014) also presented the idea of adding more supervision by matching the intermediate representation using regressors. Yim et al. (Yim et al. 2017) formulated the distillation problem using the flow of solution procedure (FSP), which is computed as the gram matrix of features across layers. Sau et al. (Sau and Balasubramanian 2016) proposed to include a noise-based regularizer while training the student with the teacher. Specifically, they perform perturbation in the logits of the teacher as a regularization approach. In Correlation Congruence for Knowledge Distillation (CCKD) (Peng et al. 2019), the authors present a framework which transfers not only instance-level information but also the correlation between instances. In CCKD, a Taylor series expansion-based kernel method is proposed to better capture the correlation between instances. Tung et al. (Tung and Mori 2019) propose a loss that is based on the observation that semantically similar inputs produce similar activation patterns in trained networks. Variational Information Distillation (VID) (Ahn et al. 2019) uses a variational lower-bound for the mutual information between the teacher and the student representations by approximating an intractable conditional distribution using a pre-defined variational distribution.

Recent works have proposed to cast knowledge distillation as a mutual information maximization problem. Contrastive representation distillation (CRD) (Tian, Krishnan, and Isola 2019) used a contrastive objective similar to Oord et al. (Oord, Li, and Vinyals 2018) to maximize a lower-bound on mutual information between final representations. The objective used by CRD is a strong lower-bound on the mutual information but requires a significant number of negative samples during training, consequently, requiring large batch-sizes or memory buffers. These practical constraints become even more limiting if mutual information needs to be minimized at the feature-level to enforce regional-supervision during student training.

Mutual Information Estimation. Mutual information is a fundamental quantity that measures the relationship between random variables which is notoriously difficult to measure (Paninski 2003). An exact estimate is only tractable

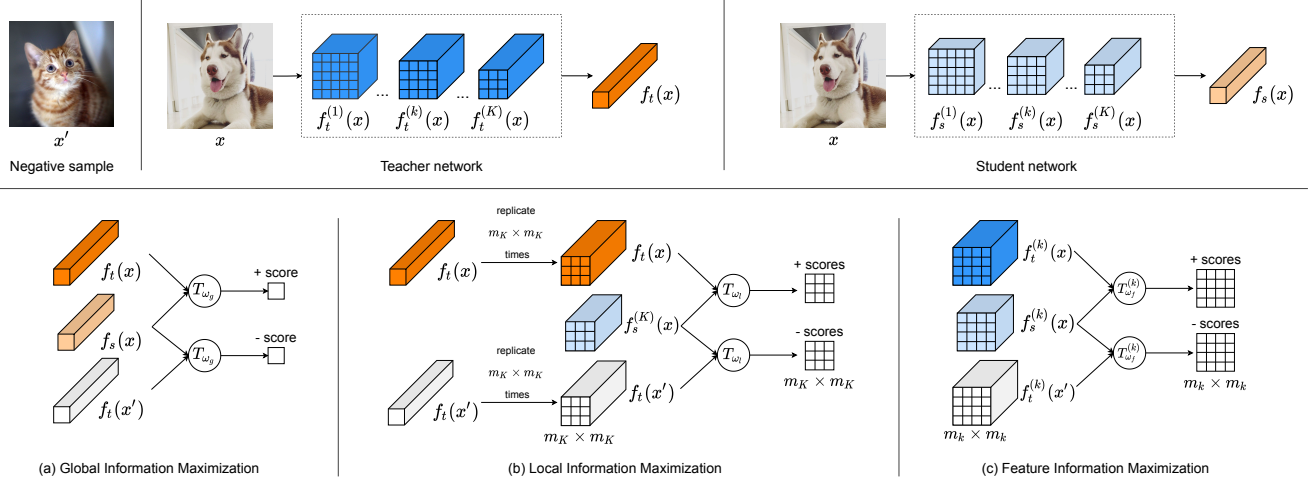


Figure 2: Overall schematic of the proposed mutual information maximization based knowledge distillation (MIMKD). **Top:** Representations generated by teacher and student networks for image x and a negative sample x' . Note that our method uses only one negative sample. **Bottom:** (a) Positive and negative pairs of final feature vectors are passed into the discriminator function to get scores. (b) Teacher’s final representation is replicated to match student’s last intermediate representation. (c) For each group of same-sized intermediate feature maps in set \mathcal{R} , positive and negative pairs are passed into a distinct discriminator function to get scores. The positive and negative scores obtained are then used with equation (2) to estimate and maximize a lower-bound on mutual information for each formulation.

for discrete variables or a small set of problems where the probability distributions are known. However, both the mentioned scenarios are unlikely for real-world visual datasets. Recently, Mutual Information Neural Estimation (MINE) (Belghazi et al. 2018) demonstrated a strong method for estimation of mutual information between high-dimensional continuous random variables using neural networks and gradient descent. MINE (Belghazi et al. 2018) proposed a general-purpose parametric neural estimator of mutual information based on dual representations of the KL-divergence (Ruderman et al. 2012). Following from MINE (Belghazi et al. 2018), Deep InfoMax (Hjelm et al. 2018) proposed a mutual information based objective for unsupervised representation learning. Deep InfoMax (Hjelm et al. 2018) contends that it is unnecessary to use the exact KL-divergence based formulation of mutual information and demonstrated the use of an alternative formulation based on the Jensen-Shannon divergence (JSD). The authors showed that the JSD based estimator is stable, and does not require a large number of negative samples. In addition, Deep InfoMax (Hjelm et al. 2018) also demonstrated the value of including global and local structure-based mutual information objectives for representation learning.

3 Method

In this section, we describe our general framework for model compression or knowledge distillation in a teacher student setup. Consider a stronger teacher network $f_t : X \rightarrow Y$ with trained parameters ϕ and a student network, operating on the same domain, $f_s : X \rightarrow Y$ with parameters θ . Let x be the sample drawn from the data distribution $p(x)$ and $f_t(x)$ & $f_s(x)$ denote the representations extracted from

the pre-classification layer, while $f_t^{cls}(x)$ & $f_s^{cls}(x)$ denote the predicted class-probability distributions from the teacher and the student networks respectively. Now consider a set $\mathcal{R} = \{(f_t^{(k)}(x), f_s^{(k)}(x))\}_{k=1}^K$ that contains K pairs of intermediate representations extracted from the networks such that each pair in the set \mathcal{R} contains same-sized intermediate representations extracted from the networks, where $m_k \times m_k$ is the size corresponding to the k -th pair in the set. Each location in these 2-dimensional intermediate representations corresponds to a specific region in the input image. Note that we do not include the final representations $f_t(x)$ and $f_s(x)$ in the set \mathcal{R} .

Our method focuses on maximizing the mutual information, (1) between final image representations $f_t(x)$ and $f_s(x)$ (global information maximization), (2) between the global image representation from the teacher network $f_t(x)$ and the last intermediate representation from the student network $f_s^{(K)}(x)$ (local information maximization), and (3) between the pairs in set \mathcal{R} (feature information maximization).

3.1 Mutual Information Maximization

In order to estimate and maximize mutual information between random variables X and Z , we train a neural network to distinguish samples generated from the joint distribution, $P(X, Z)$ and the product of marginals $P(X)P(Z)$. In MINE (Belghazi et al. 2018), the authors use the Donsker-Varadhan (Donsker and Varadhan 1983) representation of the KL-divergence as the lower bound on the mutual information,

Teacher Student	WRN-40-2 WRN-16-1	WRN-40-2 WRN-16-2	resnet110 resnet8	resnet110 resnet20	resnet56 resnet20	resnet32x4 resnet8x4	vgg19 vgg8
Teacher baseline	75.31	75.31	73.82	73.82	72.31	79.24	74.63
Student baseline	67.01	72.80	59.63	69.10	69.10	72.44	69.67
KD (2015)	68.24	73.91	61.01	70.32	70.59	73.21	72.29
VID (2019)	68.95	73.89	60.44	70.32	70.52	73.19	71.52
CRD (2019)	69.21	74.17	60.82	71.45	71.12	75.21	73.10
FitNet (2014)	68.35	73.11	60.36	69.12	69.28	73.80	71.32
AT (2016a)	68.49	73.37	60.24	70.36	70.18	73.20	71.71
MIMKD	70.20	75.16	61.81	71.43	71.31	75.83	73.27

Table 1: Observed test accuracy (in %) of student networks trained with teacher networks of higher capacity but similar architecture on the CIFAR100 dataset using our methods MIMKD and other distillation frameworks.

$$\begin{aligned}
I(X; Z) &:= D_{KL}(P(X, Z) \parallel P(X)P(Z)) \\
&\geq \hat{I}_\omega^{DV}(X; Z) := \mathbb{E}_{P(X, Z)}[T_\omega] \\
&\quad - \log \mathbb{E}_{P(X)P(Z)}[e^{T_\omega}], \quad (1)
\end{aligned}$$

where $T_\omega : \mathcal{X} \times \mathcal{Z} \rightarrow \mathbb{R}$ is the discriminator neural network with parameters ω .

Another popular bound on mutual information is formulated as infoNCE (Oord, Li, and Vinyals 2018) based on Noise-Contrastive Estimation (Gutmann and Hyvärinen 2010). However, as demonstrated in (Hjelm et al. 2018), both DV and infoNCE bound require a large number of negative samples during training. Recent works tackle this problem by using a memory-buffer that keeps representations from previous samples in memory to be accessed during training. As implemented in CRD (Tian, Krishnan, and Isola 2019), this can be done if mutual information is maximized only between the final representations of the networks as the dimensions of the representations to be kept in memory is limited. In our setup, we require negative samples for each location in the multiple (K) intermediate feature maps as well as for the final representations which becomes unfeasible for most large state-of-the-art architectures.

Different from above methods, in our approach we use Jensen-Shannon divergence based mutual information estimation, similar to the formulations in (Nowozin, Cseke, and Tomioka 2016) and (Brakel and Bengio 2017),

$$\begin{aligned}
I(X; Z) &\geq \hat{I}_\omega^{JSD}(X; Z) := \mathbb{E}_{P(X, Z)}[-\log(1 + e^{-T_\omega})] \\
&\quad - \log \mathbb{E}_{P(X)P(Z)}[\log(1 + e^{T_\omega})], \quad (2)
\end{aligned}$$

Overall, we optimize the parameters θ of the student network (f_s) and parameters ω of the critic network (T_ω) by simultaneously estimating & maximizing mutual information between the representations of the frozen teacher network & the student network.

3.2 Global information maximization

Our global objective aims to maximize the mutual information between the richer final representation of the frozen teacher network $f_t(x)$ and the final representation of the student network $f_s(x)$ to encourage the student to learn richer

representations. This objective uses a discriminator function T_{ω_g} , where ω_g are the trainable parameters. We optimize the parameters of the student and the discriminator function simultaneously as:

$$(\hat{\omega}_g, \hat{\theta}) = \underset{\omega_g, \theta}{\operatorname{argmax}} \hat{I}_{\omega_g}(f_t(x), f_s(x)). \quad (3)$$

3.3 Local information maximization

In this objective we maximize the mutual information between a richer final representation of the teacher network and representations of local regions extracted by the student network. This objective draws from the assertion that the final teacher representations contains valuable information required for downstream classification. Hence, this objective encourages the student network to extract information from local image regions that is ultimately useful for classification.

We enforce this objective between $f_t(x)$ and the last intermediate representation from the student network in the set \mathcal{R} . Therefore for $k = K$, $f_s^{(K)}(x)$ is a $m_K \times m_K$ feature map where each location roughly corresponds to an $H/m_K \times W/m_K$ patch in the input image where H, W are the height and width of the image. Representation of each such patch $\{f_s^{(K)}(x)\}_{i,j}$ is then paired with $f_t(x)$, where $i, j \in [1, m_K]$ denote the specific location in the feature map. The pairs are then used with the mutual information estimator to optimize the parameters as follows:

$$(\hat{\omega}_l, \hat{\theta}) = \underset{\omega_l, \theta}{\operatorname{argmax}} \frac{1}{m_K^2} \sum_{i=1}^{m_K} \sum_{j=1}^{m_K} \hat{I}_{\omega_l}(f_t(x), \{f_s^{(K)}(x)\}_{i,j}), \quad (4)$$

where discriminator neural network T_{ω_l} with parameters ω_l is used.

3.4 Feature Information maximization

This objective aims to maximize the mutual information between region-consistent intermediate representations from the networks. In neural networks, the complexity of captured visual patterns increases towards the later layers (Zeiler and Fergus 2014). Intuitively, to mimic the representational power of the teacher, the student network needs to learn

Teacher Student	resnet110 WRN-16-1	resnet32x4 WRN-16-2	resnet32x4 vgg8	vgg13 ShuffleNetV1	ResNet50 ShuffleNetV2	vgg13 MobileNetV2
Teacher baseline	73.82	79.24	79.24	74.62	79.23	74.62
Student baseline	67.01	72.80	69.67	70.51	69.85	61.11
KD (2015)	68.86	74.63	73.46	72.26	72.91	64.47
VID (2019)	67.47	73.38	71.52	72.22	72.84	63.01
CRD (2019)	69.71	75.61	73.73	72.86	73.65	66.34
FitNet (2014)	67.99	73.79	70.28	72.29	71.80	61.42
AT (2016a)	66.42	72.19	71.77	71.19	70.78	61.96
MIMKD	69.88	76.24	74.09	73.88	74.55	65.89

Table 2: Observed test accuracy (in %) of student networks trained with teacher networks of higher capacity and different architecture on the CIFAR100 dataset using our method MIMKD and other distillation frameworks.

these complex patterns hierarchically. In order to motivate such hierarchical learning, mutual information is maximized between intermediate features at different depths in the networks. This enables the student to learn to identify complex patterns in a bottom-up fashion and systematically learn to generate richer features. Note that within each pair of intermediate feature maps in set \mathcal{R} , mutual information is maximized between vectors corresponding to the same location in the image. This information maximization pushes the student network to extract features from each region of the image that shares maximum information with the features extracted by the teacher network from the same region. Now for a pair $(f_t^{(k)}(x), f_s^{(k)}(x)) \in \mathcal{R}$, information is maximized between pairs of region-consistent vectors $\{f_t^{(k)}(x)\}_{i,j}$ and $\{f_s^{(k)}(x)\}_{i,j}$ for each $i, j \in [1, m_k]$ as follows:

$$(\hat{\omega}_f, \hat{\theta}) = \underset{\omega_f, \theta}{\operatorname{argmax}} \frac{1}{K} \frac{1}{m_k^2} \sum_{k=1}^K \sum_{i=1}^{m_k} \sum_{j=1}^{m_k} \hat{I}_{\omega_f}(\{f_t^{(k)}(x)\}_{i,j}, \{f_s^{(k)}(x)\}_{i,j}),$$

where discriminator neural network T_{ω_f} with parameters ω_f is used.

3.5 Divergence objective

This objective aims to minimize the divergence between the predicted class-probability distributions from teacher and student models. In order to do this, KD (Hinton, Vinyals, and Dean 2015) minimizes the Kullback-Leibler divergence (KLD). However, KL-divergence serves as poor distance-metric due to its non-symmetric nature. Therefore, we formulate an objective based on the Jensen-Shannon Divergence (JSD) to measure the similarity between probability distributions. Overall, due to the favorable properties of JSD over KLD, our objective is a symmetric and smoothed version of the its KLD-based counterpart and can be used as a distance metric.

Mathematically, we minimize the divergence between the output probability distributions $f_t^{cls}(x)$ and $f_s^{cls}(x)$, from the teacher and the student, using the following objective:

$$(\hat{\theta}) = \underset{\theta}{\operatorname{argmin}} \frac{KL(f_t^{cls}(x) \parallel Q)}{2} + \frac{KL(f_s^{cls}(x) \parallel Q)}{2},$$

where,

$$Q = \frac{f_t^{cls}(x) + f_s^{cls}(x)}{2} \quad (5)$$

This objective functions as label-smoothing during training by encouraging the student to mimic the softened class scores of the teacher.

3.6 Classification objective

Here the cross-entropy loss is minimized between the output of the classification function $f_s^{cls}(x)$ and the target label y as follows:

$$(\hat{\theta}) = \underset{\theta}{\operatorname{argmin}} \mathcal{L}_{CE}(y, f_s^{cls}(x)), \quad (6)$$

where \mathcal{L}_{CE} denotes the cross-entropy function.

Our overall objective is a weighted-summation of all the above individual objectives with weights α (cross-entropy loss), $1 - \alpha$ (JS-divergence objective), λ_g (global MI maximization), λ_l (local MI maximization), and λ_f (feature MI maximization)

4 Experiments

We evaluate the performance of our approach on the task of model compression on the CIFAR-100 dataset (Krizhevsky, Hinton et al. 2009) in two distinct setups. First, we perform model compression between pairs of (1) similar standard CNN architectures of varying capacities and (2) between pairs of significantly different standard CNN architectures. Second, we perform model compression via knowledge distillation from a standard CNN architectures to shallower self-designed CNN architectures. The CIFAR-100 dataset contains colored natural images of size 32×32 . It has 50K training images with 500 images in each of the 100 classes and a total of 10K test images. In our experiments, we use the standard CNN architectures of varied capacities, such as

Teacher Student	resnet110 Conv-4	resnet32x4 Conv-4	vgg13 Conv-4	resnet110 Conv-4-MP	resnet32x4 Conv-4-MP	vgg13 Conv-4-MP
Teacher baseline	73.82	79.24	74.62	73.82	79.24	74.62
Student baseline	59.97	59.97	59.97	66.09	66.09	66.09
KD (2015)	61.98	62.87	62.10	67.51	68.04	67.84
VID (2019)	61.93	63.45	62.49	67.76	67.86	67.40
CRD (2019)	62.13	63.76	62.54	67.96	68.52	68.06
FitNet (2014)	60.58	62.89	61.81	67.38	67.21	66.52
AT (2016a)	61.65	63.10	62.16	67.52	66.03	66.21
MIMKD	62.91	64.32	62.95	68.77	69.09	68.91

Table 3: Observed test accuracy (in %) of shallow student networks trained with teacher networks of higher capacity and standard architectures on the CIFAR100 dataset using our methods MIMKD and other distillation frameworks.

ResNet (He et al. 2016), Wide ResNet (WRN) (Zagoruyko and Komodakis 2016b), MobileNet (Sandler et al. 2018), ShuffleNet (Zhang et al. 2018), and VGG (Simonyan and Zisserman 2014).

We compare our method with other knowledge distillation methods, such as (1) Knowledge Distillation (KD) (Hinton, Vinyals, and Dean 2015), (2) FitNets (Romero et al. 2014), (3) Attention Transfer (AT) (Zagoruyko and Komodakis 2016a), (4) Variational Information Distillation (VID) (Ahn et al. 2019), and (5) Contrastive Representation Distillation (CRD) (Tian, Krishnan, and Isola 2019) based on classification performance on the CIFAR-100 testset. Ablative study was performed to find optimal values of hyper-parameters; we set, $\alpha = 0.9$, $\lambda_g = 0.2$, $\lambda_l = 0.8$, $\lambda_f = 0.8$ for all our experiments. The hyper-parameter choice for other approaches can be found in the appendix.

Additionally, in order to demonstrate the scalability of our method, we compare our distillation performance on the ImageNet (Deng et al. 2009) dataset against AT (Zagoruyko and Komodakis 2016a), and KD (Hinton, Vinyals, and Dean 2015). ImageNet is a large-scale dataset with 1.2 million training images across 1K classes and a total of 50K validation images.

4.1 Implementation Details

We adopted the generally established approach for training CNNs on the CIFAR-100 dataset. We use SGD with momentum 0.9, weight decay 5×10^{-4} , and an initial learning rate of 0.05 for a total of 240 epochs with batch-size 64. The learning rate is decayed by 0.1 every at the 150, 180 and the 210-th epoch. We used random horizontal flips and random crop for augmenting the dataset during training. For ImageNet, we use the standard PyTorch training scheme for training a ResNet (He et al. 2016).

The parameterized mutual information discriminator functions (T_{ω_g} , T_{ω_l} , & T_{ω_f}) can be modeled by arbitrary neural networks. In our experiments, we use two distinct architectures described in detail in the appendix A.3.

4.2 Results

In this section we demonstrate the prowess of our distillation framework using model compression performance in the following setups.

Similar CNN Architectures. We perform knowledge distillation from a teacher network to a student network of the same family. It can be seen (ref. Table 1) that our method outperforms other methods in most setups. Notice that CRD (Tian, Krishnan, and Isola 2019) is able to slightly surpass the performance of our method in one setup while being close in most cases. We find this encouraging as CRD (Tian, Krishnan, and Isola 2019) uses a similar mutual information maximization based formulation in their distillation objective with a tighter lower-bound. Therefore, if we only use the global objective in our method, CRD (Tian, Krishnan, and Isola 2019) should generally outperform our method owing to its tighter bound. The fact that our approach gives competitive performance with CRD (Tian, Krishnan, and Isola 2019) despite compromising the lower bound on mutual information, demonstrates the overall value of using region-consistent local and feature-level mutual information maximization schemes.

Dissimilar CNN Architectures. Here, we perform knowledge distillation from a teacher network to a student network with a significantly different architecture. This tests the flexibility of our method to adapt to distinct data-abstraction flows of dissimilar neural network architectures. Table 2 demonstrates that our method (MIMKD) outperforms other distillation methods in most teacher-student combinations increasing the accuracy of a ShuffleNetV2 by 4.7% while distilling from a much different ResNet50 model. This demonstrates that our method is able to accommodate significant architectural differences in teacher-student pairs and does not impose structural constraints on intermediate layers that hinder training. While other methods that work on intermediate feature maps like AT (Zagoruyko and Komodakis 2016a) and Fitnets (Romero et al. 2014) perform worse than baseline.

Shallow CNN Architectures. In this section, we describe our experiments where we distill knowledge from a standard teacher network into a shallow self-designed CNN. This is done to demonstrate that it is feasible to design and distill information into light-weight models such that they perform competitively with standard CNN architectures while running faster. For our experiments we use 2 shallow CNNs; (1) Conv-4 with 4 convolutional-blocks followed by

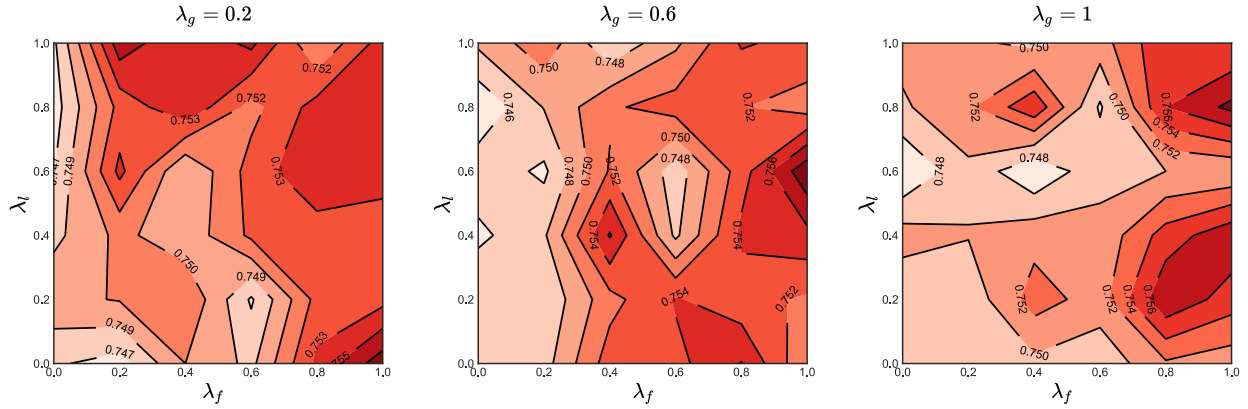


Figure 3: Results from the ablation studies on CIFAR100 dataset using a student resnet8x4 (baseline acc. 72.44%) with teacher resnet32x4 (baseline acc. 79.24%). Contour lines represent the final test accuracy of the student. Grid search was performed by varying the values of λ_f , λ_g , λ_l from 0 to 1 with increments of 0.2 while α was kept constant at 1. In each plot, the accuracy landscape is shown with λ_g set to a constant value. Plots for remaining values of λ_g have been added to the appendix.

average pooling operation and a linear layer, where each convolutional-block is made-up of a convolutional layer with kernel size 3×3 and stride 2 followed by batch-normalization and a ReLU non-linearity, (2) Conv-4-MP which has 4 convolutions blocks followed by average pooling and a linear layer at the end, where each convolutional-block contains a convolutional layer with kernel size 3×3 and stride 1 followed by batch-normalization, ReLU and a max-pooling layer. These architectures were chosen as they are compact and run relatively faster on standard CPUs (ref. Figure 1). Table 3 compiles our results compared to other distillation methods for self-designed shallow CNN architectures. Our method is able to outperform all other methods in this setup. Additionally, we can see that distillation is most successful with resnet32x4 as the teacher than for other architectures. This could be because of the larger gap in the baseline accuracy of the networks.

ImageNet results. In this experiment we train a student ResNet-18 with a pre-trained teacher ResNet-34 on the ImageNet dataset. Note that we do not perform any hyper-parameter tuning specifically for this configuration and use the same values we obtained for the CIFAR-100 dataset i.e. $\alpha = 0.9$, $\lambda_g = 0.2$, $\lambda_l = 0.8$, $\lambda_f = 0.8$. We observed that our method is able to reduce the gap between the teacher and the student performance by 1.44%.

4.3 Ablation Study

We perform an extensive ablation study to demonstrate the value of each component of our mutual information maximization objective. Ablative study experiments are performed with the teacher network resnet32x4 and the student network resnet8x4 where the baseline accuracy of the teacher is 79.24% and that of the student network is 72.44%. The values of the hyper-parameters λ_g , λ_l and λ_f — that control the weight of the global, local and feature mutual information maximization objectives respectively — were var-

Teacher	ResNet-34
Student	ResNet-18
Teacher baseline	72.82
Student baseline	68.88
KD (2015)	69.66
AT (2016a)	69.70
MIMKD	70.32

Table 4: Observed Top-1 validation accuracy (in %) of the student network on the ImageNet dataset using our method (MIMKD) and other distillation frameworks.

ied between 0 and 1 with an increment of 0.2. The contour plots in Figure 6 shows the test accuracy landscape with respect to the values of the hyper-parameters. It can be seen from the figure that for any value of λ_g , we can observe generally higher performance towards higher values of λ_f . This shows the value of maximizing region-consistent mutual information between representations. Please refer to the appendix for additional accuracy landscape plots.

5 Conclusions

In this paper, we presented a novel Mutual Information Maximization based knowledge distillation framework (MIMKD). Our method was formulated using the JSD based lower-bound on mutual information which we optimize using only one negative sample. We presented three information maximization formulations and demonstrated the value of region-consistent information maximization on distillation performance. Further works could explore our contention that if used with a tighter lower-bound, our information maximization objectives have the potential to surpass even its current performance. The role and the architecture of the discriminator functions can also be explored further in future works.

References

- Ahn, S.; Hu, S. X.; Damianou, A.; Lawrence, N. D.; and Dai, Z. 2019. Variational information distillation for knowledge transfer. In *Proceedings of the IEEE/CVF Conference on Computer Vision and Pattern Recognition*, 9163–9171.
- Belghazi, M. I.; Baratin, A.; Rajeshwar, S.; Ozair, S.; Bengio, Y.; Courville, A.; and Hjelm, D. 2018. Mutual information neural estimation. In *International Conference on Machine Learning*, 531–540. PMLR.
- Brakel, P.; and Bengio, Y. 2017. Learning independent features with adversarial nets for non-linear ica. *arXiv preprint arXiv:1710.05050*.
- Buciluă, C.; Caruana, R.; and Niculescu-Mizil, A. 2006. Model compression. In *Proceedings of the 12th ACM SIGKDD international conference on Knowledge discovery and data mining*, 535–541.
- Chen, G.; Choi, W.; Yu, X.; Han, T.; and Chandraker, M. 2017. Learning efficient object detection models with knowledge distillation. In *Proceedings of the 31st International Conference on Neural Information Processing Systems*, 742–751.
- Chen, T.; Kornblith, S.; Norouzi, M.; and Hinton, G. 2020. A simple framework for contrastive learning of visual representations. In *International conference on machine learning*, 1597–1607. PMLR.
- Deng, J.; Dong, W.; Socher, R.; Li, L.-J.; Li, K.; and Fei-Fei, L. 2009. Imagenet: A large-scale hierarchical image database. In *2009 IEEE conference on computer vision and pattern recognition*, 248–255. Ieee.
- Donsker, M. D.; and Varadhan, S. S. 1983. Asymptotic evaluation of certain Markov process expectations for large time. IV. *Communications on Pure and Applied Mathematics*, 36(2): 183–212.
- Gutmann, M.; and Hyvärinen, A. 2010. Noise-contrastive estimation: A new estimation principle for unnormalized statistical models. In *Proceedings of the Thirteenth International Conference on Artificial Intelligence and Statistics*, 297–304. JMLR Workshop and Conference Proceedings.
- He, K.; Fan, H.; Wu, Y.; Xie, S.; and Girshick, R. 2020. Momentum contrast for unsupervised visual representation learning. In *Proceedings of the IEEE/CVF Conference on Computer Vision and Pattern Recognition*, 9729–9738.
- He, K.; Zhang, X.; Ren, S.; and Sun, J. 2016. Deep residual learning for image recognition. In *Proceedings of the IEEE conference on computer vision and pattern recognition*, 770–778.
- Hinton, G.; Vinyals, O.; and Dean, J. 2015. Distilling the knowledge in a neural network. *arXiv preprint arXiv:1503.02531*.
- Hjelm, R. D.; Fedorov, A.; Lavoie-Marchildon, S.; Grewal, K.; Bachman, P.; Trischler, A.; and Bengio, Y. 2018. Learning deep representations by mutual information estimation and maximization. *arXiv preprint arXiv:1808.06670*.
- Huang, Z.; and Wang, N. 2018. Data-driven sparse structure selection for deep neural networks. In *Proceedings of the European conference on computer vision (ECCV)*, 304–320.
- Krizhevsky, A.; Hinton, G.; et al. 2009. Learning multiple layers of features from tiny images.
- Nowozin, S.; Cseke, B.; and Tomioka, R. 2016. f-gan: Training generative neural samplers using variational divergence minimization. *arXiv preprint arXiv:1606.00709*.
- Oord, A. v. d.; Li, Y.; and Vinyals, O. 2018. Representation learning with contrastive predictive coding. *arXiv preprint arXiv:1807.03748*.
- Paninski, L. 2003. Estimation of entropy and mutual information. *Neural computation*, 15(6): 1191–1253.
- Peng, B.; Jin, X.; Liu, J.; Li, D.; Wu, Y.; Liu, Y.; Zhou, S.; and Zhang, Z. 2019. Correlation congruence for knowledge distillation. In *Proceedings of the IEEE/CVF International Conference on Computer Vision*, 5007–5016.
- Romero, A.; Ballas, N.; Kahou, S. E.; Chassang, A.; Gatta, C.; and Bengio, Y. 2014. Fitnets: Hints for thin deep nets. *arXiv preprint arXiv:1412.6550*.
- Ruderman, A.; Reid, M.; García-García, D.; and Petterson, J. 2012. Tighter variational representations of f-divergences via restriction to probability measures. *arXiv preprint arXiv:1206.4664*.
- Sandler, M.; Howard, A.; Zhu, M.; Zhmoginov, A.; and Chen, L.-C. 2018. Mobilenetv2: Inverted residuals and linear bottlenecks. In *Proceedings of the IEEE conference on computer vision and pattern recognition*, 4510–4520.
- Sau, B. B.; and Balasubramanian, V. N. 2016. Deep model compression: Distilling knowledge from noisy teachers. *arXiv preprint arXiv:1610.09650*.
- Simonyan, K.; and Zisserman, A. 2014. Very deep convolutional networks for large-scale image recognition. *arXiv preprint arXiv:1409.1556*.
- Tian, Y.; Krishnan, D.; and Isola, P. 2019. Contrastive representation distillation. *arXiv preprint arXiv:1910.10699*.
- Tung, F.; and Mori, G. 2019. Similarity-preserving knowledge distillation. In *Proceedings of the IEEE/CVF International Conference on Computer Vision*, 1365–1374.
- Wu, Z.; Xiong, Y.; Yu, S. X.; and Lin, D. 2018. Unsupervised feature learning via non-parametric instance discrimination. In *Proceedings of the IEEE conference on computer vision and pattern recognition*, 3733–3742.
- Yim, J.; Joo, D.; Bae, J.; and Kim, J. 2017. A gift from knowledge distillation: Fast optimization, network minimization and transfer learning. In *Proceedings of the IEEE Conference on Computer Vision and Pattern Recognition*, 4133–4141.
- Zagoruyko, S.; and Komodakis, N. 2016a. Paying more attention to attention: Improving the performance of convolutional neural networks via attention transfer. *arXiv preprint arXiv:1612.03928*.
- Zagoruyko, S.; and Komodakis, N. 2016b. Wide residual networks. *arXiv preprint arXiv:1605.07146*.
- Zeiler, M. D.; and Fergus, R. 2014. Visualizing and understanding convolutional networks. In *European conference on computer vision*, 818–833. Springer.

Zhang, F.; Zhu, X.; and Ye, M. 2019. Fast human pose estimation. In *Proceedings of the IEEE/CVF Conference on Computer Vision and Pattern Recognition*, 3517–3526.

Zhang, X.; Zhou, X.; Lin, M.; and Sun, J. 2018. Shufflenet: An extremely efficient convolutional neural network for mobile devices. In *Proceedings of the IEEE conference on computer vision and pattern recognition*, 6848–6856.

A Appendix

A.1 Hyper-parameters for other methods

The student is trained with the following loss function which is a combination of the distillation loss and the cross-entropy loss for classification:

$$\mathcal{L} = \alpha \mathcal{L}_{cls} + (1 - \alpha) \mathcal{L}_{KD} + \beta \mathcal{L}_{dis} \quad (7)$$

Note that we set $\alpha = 1$ for all methods except KD(Hinton, Vinyals, and Dean 2015) and the value of β is set to the value recommended in the original work as follows:

1. KD (Hinton, Vinyals, and Dean 2015): $\alpha = 0.9, \beta = 0$
2. Fitnet (Romero et al. 2014): $\beta = 100$
3. AT (Zagoruyko and Komodakis 2016a): $\beta = 1000$
4. VID (Ahn et al. 2019): $\beta = 1$
5. CRD (Tian, Krishnan, and Isola 2019): $\beta = 0.8$

A.2 Defining \mathcal{R}

Similar CNN Architectures. Consider the case of distillation when the teacher network is a pre-trained WRN-40-2 and the student network is a WRN-16-1. We use 4 same-sized representations extracted from intermediate layers of the networks. Therefore, the set $\mathcal{R} = \{(f_t^{(k)}(x), f_s^{(k)}(x))\}_{k=1}^K$ contains k pairs of same-sized 2-dimensional representations. Table 5 describes the sizes of the intermediate representations used for feature-based mutual information maximization. It can be seen that for this combination we use $k = 4$ in our formulation.

	WRN-40-2	WRN-16-1
k	$f_t^{(k)}(x)$	$f_s^{(k)}(x)$
1	$16 \times 32 \times 32$	$16 \times 32 \times 32$
2	$32 \times 32 \times 32$	$16 \times 32 \times 32$
3	$64 \times 16 \times 16$	$32 \times 16 \times 16$
4	$128 \times 8 \times 8$	$64 \times 8 \times 8$

Table 5: Dimensions of intermediate representation in the form *channels* \times *height* \times *width* used for feature-level mutual information maximization between a teacher WRN-40-2 and a student WRN-16-1 network. Alternatively, each value of k represents a pair of elements in the set \mathcal{R} .

Dissimilar CNN Architectures. Similar approach of defining the set \mathcal{R} is followed in cases where the teacher and student networks have significantly different architectures. For instance, Table 6 shows the dimensions of intermediate representations used when the teacher network is a ResNet34 while the student is a ShuffleNetV2. Here $k = 4$ is used, however, for some combinations of different standard architectures we use $k = 3$ if only 3 pairs intermediate representations from the teacher and the student have the same size. Note that our method is invariant to the number of channels in the representations. Therefore, mismatch in the number of channels in pairs of representations in \mathcal{R} is inconsequential for the formulation of our losses.

	ResNet34	ShuffleNetV2
k	$f_t^{(k)}(x)$	$f_s^{(k)}(x)$
1	$64 \times 32 \times 32$	$24 \times 32 \times 32$
2	$512 \times 16 \times 16$	$116 \times 16 \times 16$
3	$1024 \times 8 \times 8$	$232 \times 8 \times 8$
4	$2048 \times 4 \times 4$	$464 \times 4 \times 4$

Table 6: Dimensions of intermediate representation in the form *channels* \times *height* \times *width* used for feature-level mutual information maximization between a teacher WRN-40-2 and a student WRN-16-1 network. Alternatively, each value of k represents a pair of elements in the set \mathcal{R} .

A.3 Mutual Information Discriminators

The parameterized mutual information discriminator functions (T_{ω_g} , T_{ω_l} , and T_{ω_f}) can be modeled as neural networks. In our experiments, we use two distinct discriminator architectures inspired from the functions presented in Deep InfoMax (Hjelm et al. 2018).

Convolve Architecture. In this method, the representations from the teacher and the student are concatenated together and passed through a series of layers to get the score. For global information maximization, the final representations from both networks is concatenated together to get $[f_s(x), f_t(x)]$. This vector is then passed to a fully connected network with two 512-unit hidden layers, each followed by a *ReLU* non-linearity (ref. table 7). The output is then passed through another linear layer to obtain the final score.

Input	Operation	Output
$[f_t(x), f_s(x)]$	LL + ReLU	O_1
O_1	LL + ReLU	O_2
O_2	LL	score

Table 7: The architecture of the discriminator used for global information maximization. Here LL denotes Linear Layer and $d(v)$ refers to the number of dimensions in vector v .

For local information maximization, we replicate the final representation from the teacher $f_t(x)$ to match the $m_K \times m_K$ size of the student’s last intermediate feature map ($f_s^{(K)}(x)$). The resulting replicated tensor is then concatenated with $f_s^{(K)}(x)$ to get $[f_t(x), f_s^{(K)}(x)]$ which serves as the input for the critic function (ref. table 8).

Similarly, consider feature mutual information maximization, for each pair in the set \mathcal{R} we use a distinct discriminator $T_{\omega_f}^{(k)}$. For a given k , each pair of intermediate feature representations in the set \mathcal{R} are concatenated together to get $[f_t^{(k)}(x), f_s^{(k)}(x)]$. Which is then passed through two convolutional (1×1 kernels and 512 filters) where each layer is followed by a *ReLU* non-linearity. The output obtained is then further passed into a convolutional layer (1×1 kernels and 1 filter) to give $m_k \times m_k$ scores (ref. table 8).

Input	Operation	Output
$[f_t(x), f_s^{(K)}(x)]$	1×1 Conv + ReLU	O_1
O_1	1×1 Conv + ReLU	O_2
O_2	1×1 Conv	scores

Table 8: The architecture of the discriminator used for local and feature mutual information maximization. Note that for feature mutual information maximization the input at the first layer is $[f_t^{(k)}(x), f_s^{(k)}(x)]$.

Project and Dot Architecture. In this method, the representations from both the teacher and the student are first projected using an appropriate projection architecture with a linear shortcut. The dot-product of these projections is then computed to get the score. Positive and negative pairs of representations are passed through the discriminator to get respective scores to be passed into equation (2) to get the estimates on the lower bound of the mutual information. One-dimensional representations are projected using the architecture described in table 9, whereas for two-dimensional intermediate feature maps, projection architecture described in table 10 is used.

Input	Operation	Output
$f_t(x)$ or $f_s(x)$	LL + ReLU + LL	O_1
$f_t(x)$ or $f_s(x)$	LL + ReLU	O_2
$O_1 + O_2$	LN	$proj$

Table 9: The projection architecture used for one-dimensional inputs. Here, LL denotes linear layer while LN denotes layer normalization. Both $f_t(x)$ and $f_s(x)$ are projected using this architecture and their dot product is computed to get scores.

Therefore, for (1) global information maximization, both $f_t(x)$ and $f_s(x)$ are projected using the one-dimensional projection architecture, for (2) local information maximization, the final teacher representation, $f_t(x)$, is projected using the one-dimensional projection architecture and duplicated to match the size of the projected intermediate student representation projected using the two-dimensional projection architecture, a dot product of these outputs is then computed to get the scores, while for (3) feature information maximization, both representations in each pair of the set \mathcal{R} is projected using a respective two-dimensional projection architecture.

Input	Operation	Output
$f_s^{(k)}(x)$	1×1 Conv + ReLU + LL	O_1
$f_s^{(k)}(x)$	1×1 Conv + ReLU	O_2
$O_1 + O_2$	LN	$proj$

Table 10: The projection architecture used for two-dimensional inputs. Here, LL denotes linear layer while LN denotes layer normalization.

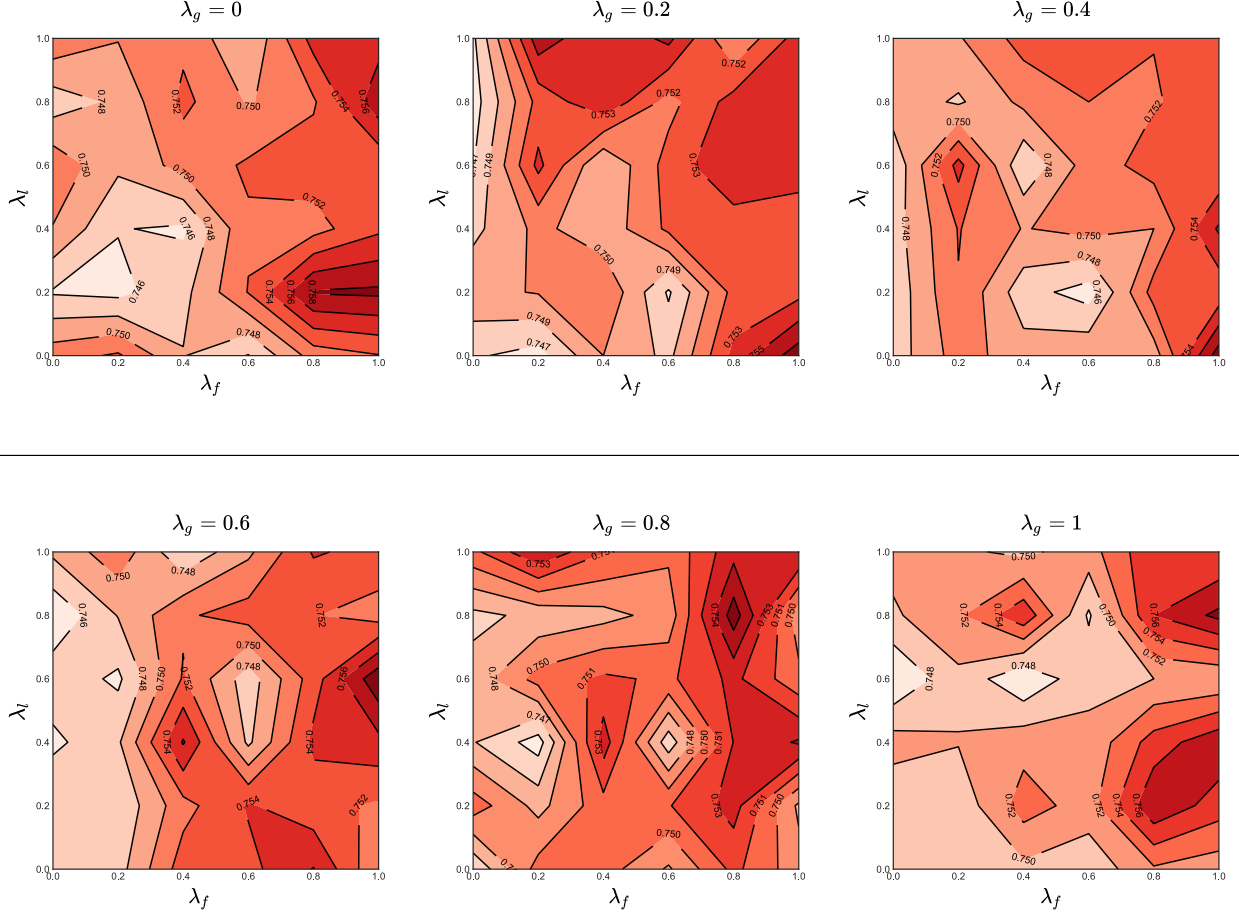


Figure 4: Results from the ablation studies on CIFAR100 dataset using a student resnet8x4 (baseline acc. 72.44%) with teacher resnet32x4 (baseline acc. 79.24%). Contour lines represent the final test accuracy of the student. Grid search was performed by varying the values of λ_f , λ_g , λ_l from 0 to 1 with increments of 0.2. In each plot, the accuracy landscape is shown with λ_g set to a constant value.

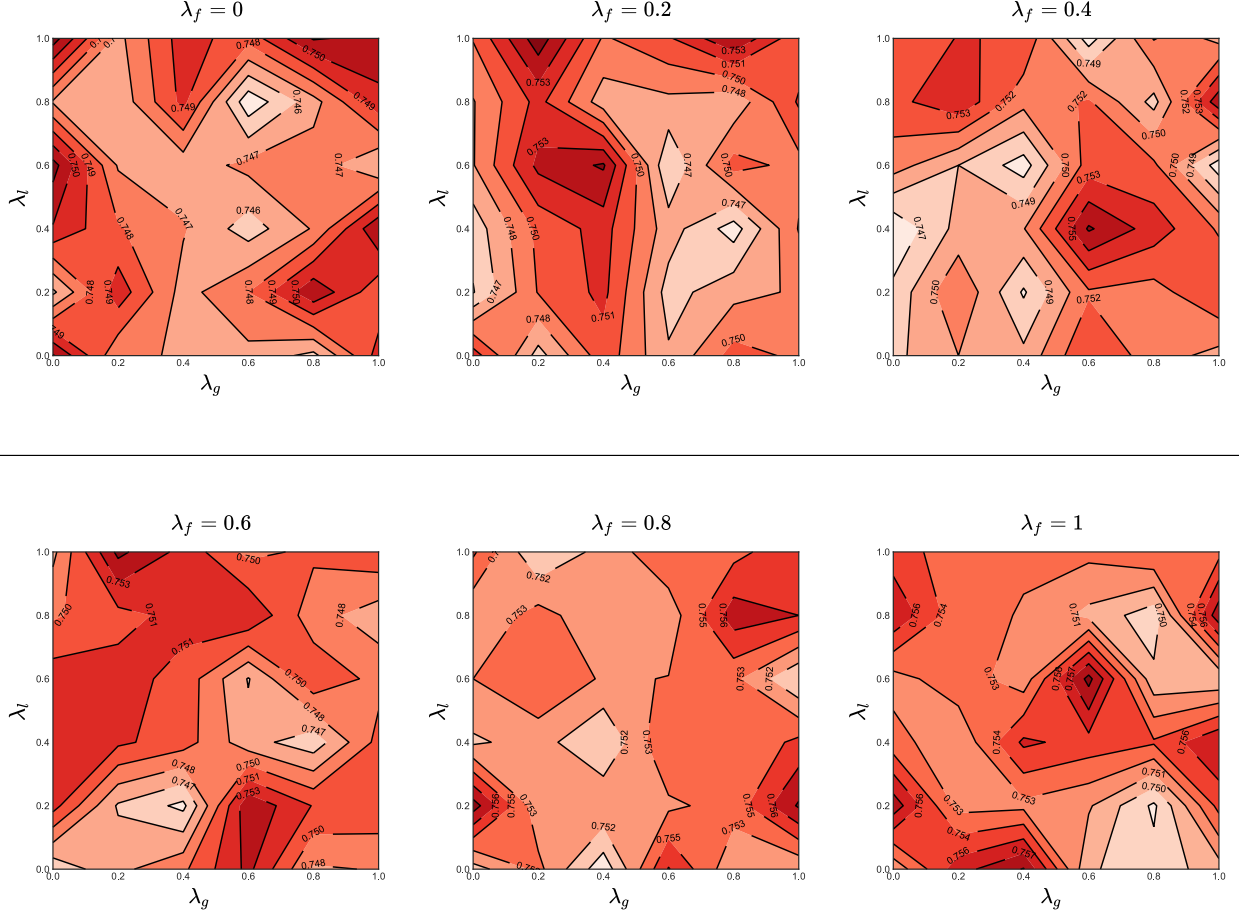


Figure 5: Results from the ablation studies on CIFAR100 dataset using a student resnet8x4 (baseline acc. 72.44%) with teacher resnet32x4 (baseline acc. 79.24%). Contour lines represent the final test accuracy of the student. Grid search was performed by varying the values of λ_f , λ_g , λ_l from 0 to 1 with increments of 0.2. In each plot, the accuracy landscape is shown with λ_f set to a constant value.

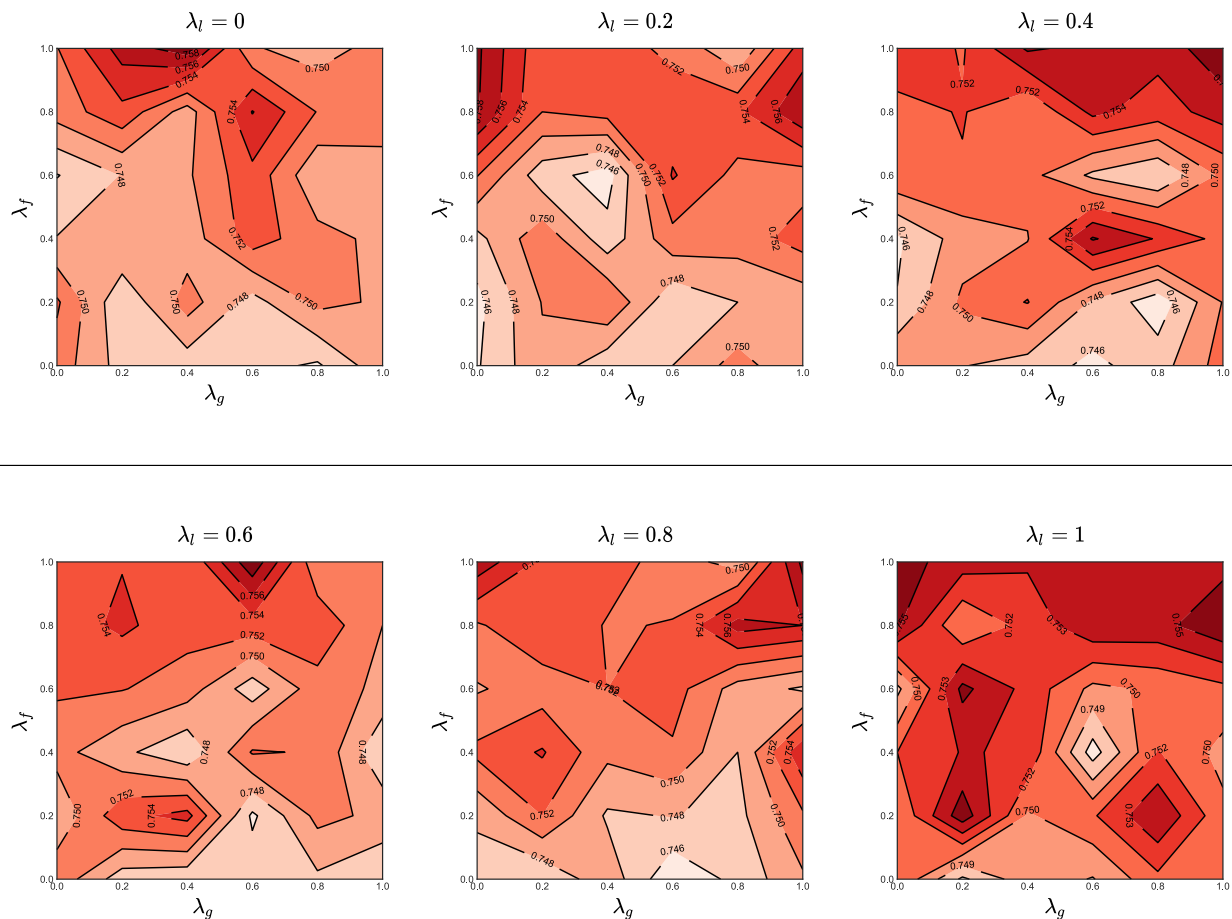


Figure 6: Results from the ablation studies on CIFAR100 dataset using a student resnet8x4 (baseline acc. 72.44%) with teacher resnet32x4 (baseline acc. 79.24%). Contour lines represent the final test accuracy of the student. Grid search was performed by varying the values of λ_f , λ_g , λ_l from 0 to 1 with increments of 0.2. In each plot, the accuracy landscape is shown with λ_l set to a constant value.